A STUDY OF RATAN-600 OBSERVATIONS OF SOLAR *S*-COMPONENT SOURCES

A. KRÜGER, J. HILDEBRANDT

Zentralinstitut für Astrophysik der Akademie der Wissenschaften der DDR, Potsdam, G.D.R.

V. M. BOGOD and A. N. KORZHAVIN

Special Astrophysical Observatory of the Academy of Sciences of the USSR, Zelenchuk, U.S.S.R.

Sh. B. AKHMEDOV and G. B. GELFREIKH

Main (Pulkovo) Observatory of the Academy of Sciences of the USSR, Leningrad, U.S.S.R.

(Received 19 June, 1985; in final form 28 February, 1986)

Abstract. A sample of 36 *S*-component sources observed by the radio telescope RATAN-600 was compared with calculations of gyromagnetic emission and bremsstrahlung based on recent sunspot models. The diagnostic possibilities of the spectral distributions in the radio flux, the degree of polarization, and the source sizes for the estimation of magnetic scale heights and other source parameters were checked by different methods.

Depending on the magnetic field structure, the observations show different types of polarization spectra. Most regular spectra and highest values of the degree of polarization were observed from sources above the leading part of the associated spot group. Magnetic scale heights were found to be intrinsically associated with the source size of the gyromagnetic emission.

The flare production rate of active regions appears to be related to their *S*-component flux and magnetic scale heights.

1. Introduction

During recent years, the investigation of solar *S*-component sources with observations of high angular resolution became a promising tool for the diagnostics of solar active regions. Since gyromagnetic radiation plays an important role for the generation of the related microwave emission, the determination of the magnetic fields at coronal heights promises a solution which otherwise is difficult to achieve.

Earlier attempts at magnetic field estimations by different methods analysing RATAN-600 data were published by Akhmedov *et al.* (1982, 1983), Bogod and Gelfreikh (1980), and Krüger *et al.* (1983). The present broader material allows a more general discussion of the question of magnetic scale heights by the study of characteristic features of the spectral distribution of the degree of polarization and other observed parameters. Furthermore, relations to optically observed structures and flare activity will be considered. Other approaches to active region magnetic fields were already described, e.g., by Schmahl *et al.* (1982) and Kundu and Alissandrakis (1984), and the current state of *S*-component analyses was discussed by Chiuderi Drago and Melozzi (1984).

Solar Physics **105** (1986) 111–121.

2. Observations

The observations used in the present paper are scans of the Sun obtained by the radio telescope RATAN-600 at 2.0, 2.3, 2.7, 3.2, and 4.0 cm wavelength (15, 13, 11, 9.4, and 7.5 GHz, respectively) attaining HPBW's of 18, 21, 25, 29, and 36 arc sec, respectively. Although this means less resolution power than reached, e.g., by the known WSRT and VLA telescopes, the RATAN observations have the advantage of yielding more spectral information and also providing integral characteristics of single active regions or characteristic parts of them. (First multiple wavelength observations of the VLA and WSRT of active regions at 2, 6, and 20 cm were published by Chiuderi Drago *et al.* (1982) and Lang *et al.* (1983).) The investigated RATAN observations were made on selected days of the years 1977–1980 where more or less compact, well separated active regions were present not very far from the centre of the solar disk. In this paper, we present for the first time an extended discussion of a total of 36 observations (cf. list of data in Table I).

3. Model Calculations

The discussion of observations is mainly based on model computations described by Krüger *et al.* (1982, 1985) and Krüger and Hildebrandt (1985). Other basically similar S-component models were elaborated by Alissandrakis *et al.* (1980) and Gelfreikh and Lubyshev (1979). Our calculations were carried out with the assumption of a horizontally stratified source volume emitting gyro-resonance (g-r) radiation and Coulomb bremsstrahlung. The source region is assumed to be embedded in the field of a magnetic dipole located at the depth $-z_d$ below the photospheric centre of a large regular sunspot. Hence, the magnetic field is described by two parameters, z_d and B_m (the latter being the maximum field at the centre of the sunspot on the photospheric level). The parameter z_d determines the magnetic scale height defined by

$$L_B(z) = B(z)\,(\mathrm{d}B(z)/\mathrm{d}z)^{-1} \tag{1}$$

(z, geometrical height above the photosphere).

For the centre of the source one obtains

$$L_B(z) = -(z + |z_d|)/3 = -z/\{3[1 - (B_m/B(z))^{-1/3}]\}\,. \tag{2}$$

Two models of the electron density and temperature distributions above sunspots have been dealt with, using the semi-empirical sunspot model by Staude (1981) which was extrapolated to coronal heights (reaching a coronal temperature T_c) with the assumption of hydrostatic equilibrium and constant conductive flux F_c (whereas F_c determines the thickness of the chromosphere-corona transition region (TR):

(a) Extended TR: $F_c = 10^4\ \mathrm{J\,m^{-2}\,s^{-1}}$, $T_c = 1.8 \times 10^6$ K.

(b) Thin TR: $F_c \approx 10^6\ \mathrm{J\,m^{-2}\,s^{-1}}$, $T_c = 2 \times 10^6$ K.

The models (a) and (b) are the same as the models A and C of Krüger *et al.* (1985), respectively; model (b) was also applied by Akhmedov *et al.* (1983) and Krüger *et al.* (1983).

TABLE I

List of RATAN-600 observations

Date	Hale No.	Pos.	$S_{7.5}$ (s.f.u.)	p_{max}	$\lambda(p_{max})$ (cm)	$R_{7.5}$ (10^6 m)	FR	Type
26 Aug., 1977	14915	26 S 07 E	1.4	0.16	2.7	2.5u	27	F
		26 S 01 E	3.3	0.28	3.2	10.7		L
24 Sep., 1977	14952	24 S 14 W	3.6	0.57	3.2	4.9	43	F
		23 S 21 W	4.2	0.81	2.3	14.2		L
5 July, 1978	15385	20 N 14 E	1.9	0.87u	2.0	20.8	12	L
21 Aug., 1978	15477	20 S 02 W	3.8	0.42	2.7	17.0	32	L
28 Jan., 1979	15786	27 S 13 W	1.1	1.00	4.0	9.6	35	L
	15788	25 S 04 E	2.6	0.62	3.2	8.6	6	L
15 Apr., 1979	15937	05 N 05 E	11.9	0.29	3.2	–	82	L
	15949	25 S 20 E	12.5	0.06	3.2	–	26	F
16 Apr., 1979	15937	03 N 10 W	17.6	0.38	3.2	34.4		L
	15949	25 S 05 E	6.6	0.80	3.2	28.0		F
1 May, 1979	15974	16 N 23 E	4.1	1.00	2.7	12.1	97	F
		16 N 11 E	5.2	0.98	2.7	10.4		L
9 May, 1979	15990	20 N 18 E	6.6	0.16	3.2	32.0	65	F
		20 N 08 E	8.4	0.43	3.2	–		L
14 July, 1979	16133	10 N 04 W	0.3	0.69	3.2	3.4	15	F
5 Oct., 1979	16337	14 N 10 W	0.7	0.10	3.2	–	25	F
		15 N 19 W	0.9	0.97	2.3	6.7		L
	16377	13 N 25 E	1.6	0.35	2.0	28.0		F
19 Jan. 1980	16601	18 S 03 E	2.0	0.19	4.0	13.9	31	F
		17 S 04 W	0.5	0.46	4.0	8.8		L
23 Apr., 1980	16789	16 S 09 E	19.0	0.95	2.7	21.4	77	L
24 Apr., 1980	16789	15 S 03 W	16.0	1.00	2.7	26.5		L
25 Apr., 1980	16789	13 S 18 W	23.0	1.00	2.3	26.5		L
27 May, 1980	16862	08 S 30 W	–	0.91	2.7	–	20	L
	16863	13 S 18 W	–	0.56	2.7	–	29	(L)
	16864	20 S 14 W	–	0.71	2.7	–	63	L
15 July, 1980	16974	17 N 04 W	1.9	0.90	3.2	6.8	53	L
	16974	19 N 01 E	2.8	0.42	4.0	7.9		L
	16978	15 S 28 E	1.9	0.06	3.2	–	124	F
		15 S 25 E	4.4	0.65	2.7	14.1		(F)
		14 S 20 E	1.9	1.00	2.7	14.1		L
29 July 1980	17008	08 S 08 E	2.0	0.32	4.0	9.1	52	L
12 Aug., 1980	17040	17 N 06 W	0.1	1.00	4.0	7.0	0	L
25 Nov., 1980	17284	20 S 03 W	0.9	0.97	2.3	3.8u,	7	L

Notes: Pos., heliographic position; FR, flare production rate during a half solar rotation (according to *Solar-Geophysical Data*, NOAA Boulder); u, uncertain; F, following part; L, leading part of associated spot group.

Diagnostic diagrams derived from the above models are shown in Figures 1(a–d): Figure 1(a) converts the flux density at a single observing frequency into couples of consistent magnetic field parameters B_m and $|z_d|$ (i.e., into B_m for any given $|z_d|$ and vice versa). In Figure 1(b) the position of the spectral maximum of the degree of circular polarization p_{max} is plotted vs B_m for different values of $|z_d|$ and both models. Figure 1(c) shows the computed source radii of g–r emission R for two selected frequencies depending on B_m and $|z_d]$. (Within the framework of accuracy of

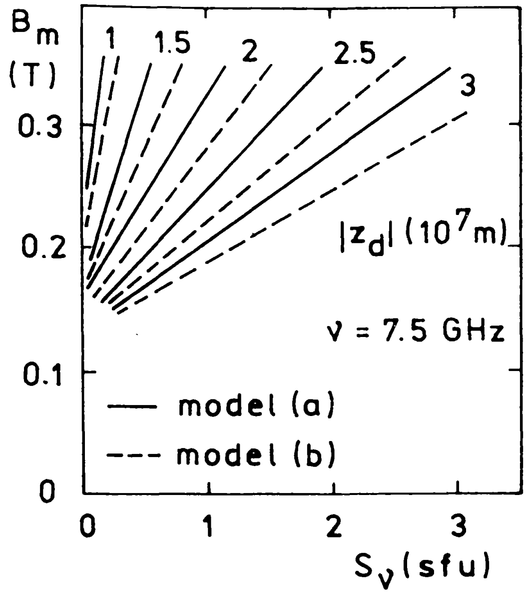

Fig. 1a.

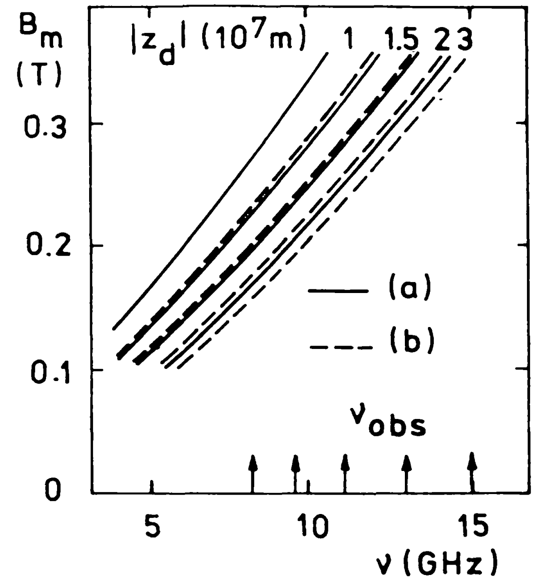

Fig. 1b.

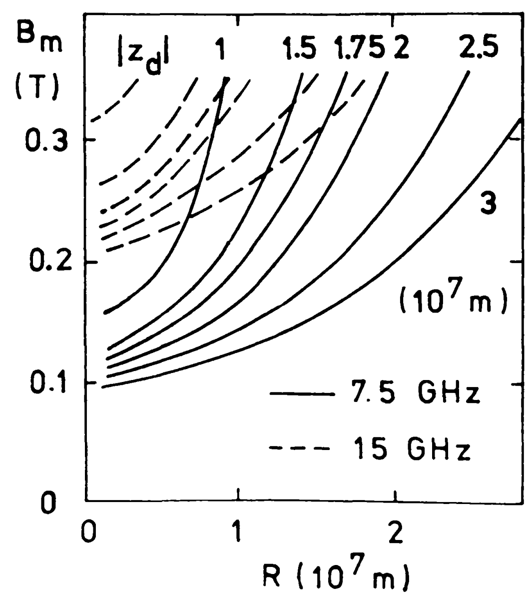

Fig. 1c.

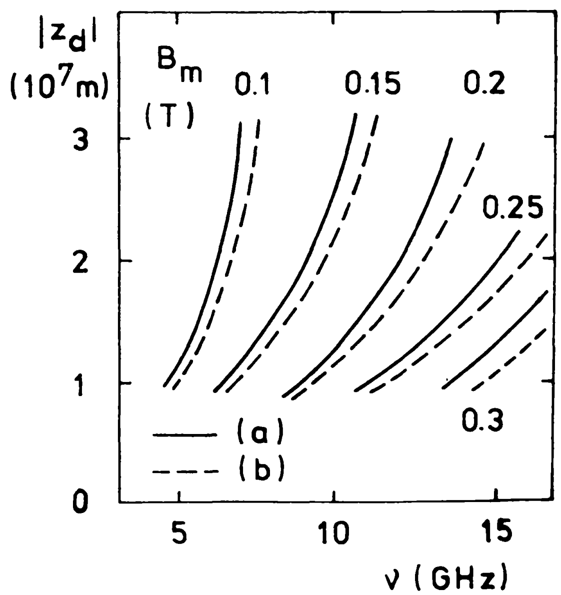

Fig. 1d.

Fig. 1. Diagnostic diagrams transforming observed S-component parameters into compatible magnetic field parameters B_m and $|z_d|$. (a) Application to the flux density S_ν at 7.5 GHz. (b) Application to the frequency of the spectral maximum of the degree of polarization $\nu(p_{\max})$. (c) Application to g–r source radii R at 7.5 and 15 GHz. (d) Application to the high-frequency edges of the spectra of the degree of polarization p.

Figure 1(c), the magnitude of R is insensitive to the choice of either model (a) or (b).) Furthermore, Figure 1(d) converts the high-frequency edges of the computed spectra of p (referring to the third harmonic of the gyrofrequency) into consistent values of B_m and $|z_d|$. More information about the full spectral dependencies of the diagnostic parameters S_ν, p, and R was given by Krüger *et al.* (1985) and Krüger and Hildebrandt (1985).

4. Spectra of the Degree of Polarization

The observations exhibit quite different spectra of $p(\nu)$, where the single maximum values p_{max} are distributed over a wide range both in p- and ν-directions (cf. Figures 2(a) and (b)). Theoretically, the spectra of p (and in particular the frequency of the spectral peaks and cut-offs) are capable of serving as an indicator of the magnetic field inside the source region (cf. Figures 1(b) and 1(d)). But in contrast to the idealized model computations which normally predict an order of $p_{max} \approx 0.9$ for g–r emission sources in the considered frequency range, a number of observations fail to show such high values of p_{max}. In principle, the deviating values of p_{max} can be considered as a signature for an inhomogeneity of the integral source region: lower values of p_{max} can be interpreted as an effect of superposition of spatially not resolved elements owing to magnetic fields of different strength and/or polarity. Furthermore, the influence of a notable contribution of bremsstrahlung can suppress the integral value of p.

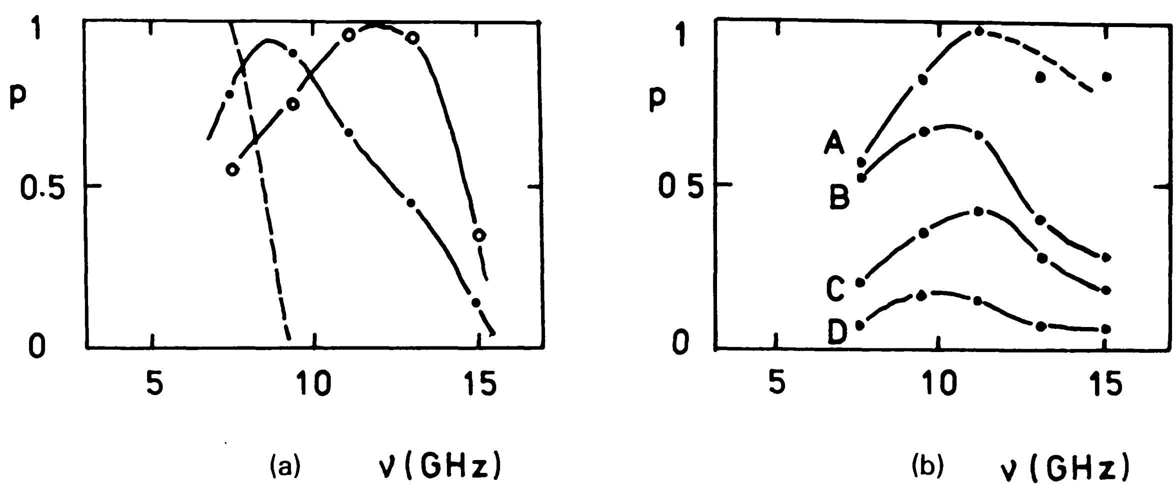

Fig. 2. Examples of observed spectra of the degree of circular polarization p of single S-component sources exhibiting different positions of the spectral maximum. (a) ---, 12 August, 1980 (AR 17040); o–o, 15 July, 1980 (AR 16974); •–•, 25 November, 1980 (AR 17284). (b) A, 1 May, 1979 (AR 15974); B, 15 July, 1980 (AR 1978), C, 21 August, 1978 (AR 15477), D, 9 May, 1979 (AR 15990).

For the purpose of a more quantitative discussion we define four groups of polarization spectra: A: $p_{max} \geq 0.8$; B: $0.8 > p_{max} \geq 0.6$; C: $0.6 > p_{max} \geq 0.4$; D: $p_{max} < 0.4$.

We found that 17 out of 20 cases belonging to the classes $A + B$ were related to the leading part of the associated spot group, and 8 out of 11 cases belonging to the class D were related to the following spots. Average values of $\nu(p_{max})$ for the classes A, B, C, and D were 11.0 ± 1.6, 9.7 ± 1.3, 9.5 ± 2.0, and 9.3 ± 1.1 GHz, respectively. The experimental results indicate the tendency that the leading part of a spot group exhibits a more homogeneous radio structure and perhaps stronger magnetic field than the following part at the height of the generation of the S-component near and above the TR.

5. Magnetic Scale Heights

Magnetic scale heights $|L_B|$ and ratios $B_m/B(z)$ related to the magnetic field near the top of the TR ($z \approx 2 \times 10^3$ km) were checked in two ways: At first we compared the observed and computed distributions of the parameters S_ν, p, and R (cf. Figures 1(a–c), Table I) and derived the best fitting average magnetic field parameters B_m and z_d (method 'B'). In doing so, no clear preference could be achieved for either model (a) or model (b). Some cases appeared to be better fitted to one or the other model, whereas the remaining cases seemed to lie in between both models.

The resulting values of $|z_d|$ vary between 1×10^7 and 3×10^7 m, with an average of the present sample of

$$|z_d| = (2.0 \pm 0.7) \times 10^7\, m$$

corresponding to a magnetic scale height (at the $z = 2 \times 10^6$ m level) of $L_B = -(7.4 \pm 2.3) \times 10^6$ m. The average values of B_m^{calc} and $B(z = 2 \times 10^6 \text{ m})$ determined by method 'B' are 0.233 and $0.175T$, respectively. For comparison, the optically observed average of B_m^{obs} (according to *Solnechnye Dannye* 33 cases were available) is $(0.239 \pm 0.05)T$ and thus accords well with the fields calculated by the radio method 'B'. Apart from the average values we compared the individual differences $\Delta B_m = |B_m^{\text{obs}} - B_m^{\text{calc}}$ case by case yielding an average of $\Delta B_m = (0.033 \pm 0.029)T$, whereas 76% and 61% of the cases exhibited $\Delta B_m \leq 0.05$ and $0.03T$, respectively. (For further comparison between B_m^{obs} and B_m^{calc}, cf. Table II).

Further, we checked the results independently with the method applied by Akhmedov *et al.* (1982) (method 'A'): here the extrapolated high-frequency edge of the spectrum of the degree of polarization is interpreted as an effect of the third harmonic of the gyrofrequency containing information on $B(z)$. Then the ratio $B_m^{\text{obs}}/B(z)$ can be deduced by means of optical observations of maximum sunspot fields. Method 'A' was applied to 27 cases (where complete optical and radio data were available) resulting in

$$B_m^{\text{obs}}/B(z) = 1.36 \pm 0.19\,.$$

This corresponds to a magnetic scale height $L_B = -6.84 \times 10^6$ m and to averages of B_m^{obs} and $B(z = 2 \times 10^6 \text{ m})$ of 0.242 and $0.178T$, respectively. These figures agree well with those obtained by the method 'B' described above.

Our results are summarized in Figure 3, where the relation between the parameters $|z_d|$, $B_m/B(z)$, and $|L_B|$ at $z = 2 \times 10^6$ m is shown. Broken lines transform the field parameters according to Equation (2) for three distinct height levels z. Full lines correspond to our models (a) and (b) where the latter (which is related to steeper gradients of the electron density and temperature, and hence to a thin TR) refers to lower effective source heights. Dots refer to source regions with different flare activity explained in Section 7. The scatter range for individual cases (four extreme points are marked by crosses in Figure 3) is partly due to observational errors as well as to real variations of the source parameters. A small systematic error, especially in method 'A', comes from the determination of the magnetic field by the third harmonic of the

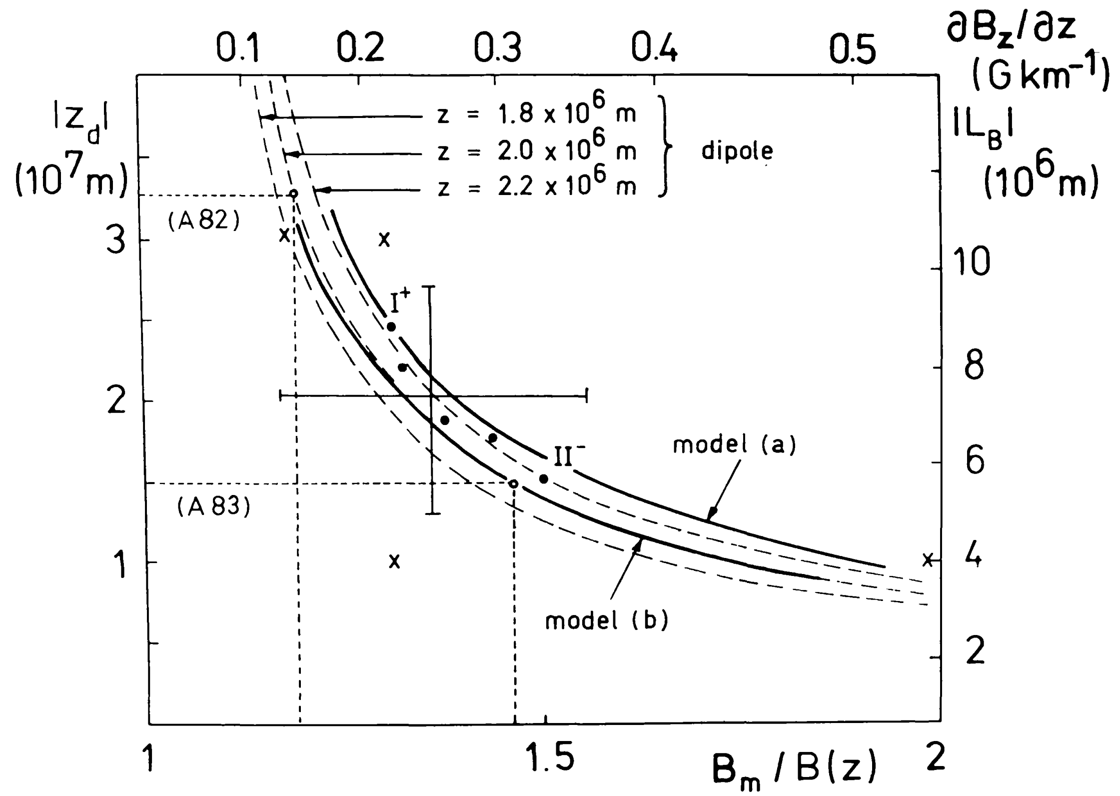

Fig. 3. Diagram illustrating the connection between various magnetic field parameters above the centre of a source region ($|z_d|$, dipole depth; $B_m/B(z)$, magnetic field ratio; $|L_B|$, magnetic scale height; $\partial B_z/\partial z$, local magnetic field gradient). Broken lines refer to dipole fields for different geometrical heights z; full lines refer to the present models (a) and (b), bars refer to an average of the computed $|z_d|$ and $B_m/B(z)$ values, crosses mark extreme outsiders of the present sample; open circles refer to samples of former papers (A82, Akhmedov *et al.*, 1982; A83, Akhmedov *et al.*, 1983); black dots refer to characteristic groups of active regions with different degree of flare activity (cf. Section 7). The scales of $|L_B|$ and $\partial B_z/\partial z$ refer to $z = 2 \times 10^6$ m; $\partial B_z/\partial z$ is taken for an average field $B_z(z) = 0.175T$.

gyrofrequency which, strictly speaking, does not refer to the source centre but to an unresolved small distance from it.

6. Source Radii

Figure 1(c) predicts a relation between the observed source radii of g–r emission and the magnetic scale heights. The result of the RATAN-600 observations is displayed by Figure 4 where the source radii at 7.5 GHz are compared with the best fitted parameters $|z_d|$. It is seen that there are no large source sizes without large magnetic scale heights. However, small source diameters occur together with small and large scale heights as well.

It should be noted that the increase of the magnetic scale height $|L_B(z = \text{const})|$ with increasing source size is not only restricted to the model of one single magnetic dipole. Also the superimposition of a number of dipoles, distributed over an area like a sunspot group, leads to an increased magnetic scale height at the base of the corona.

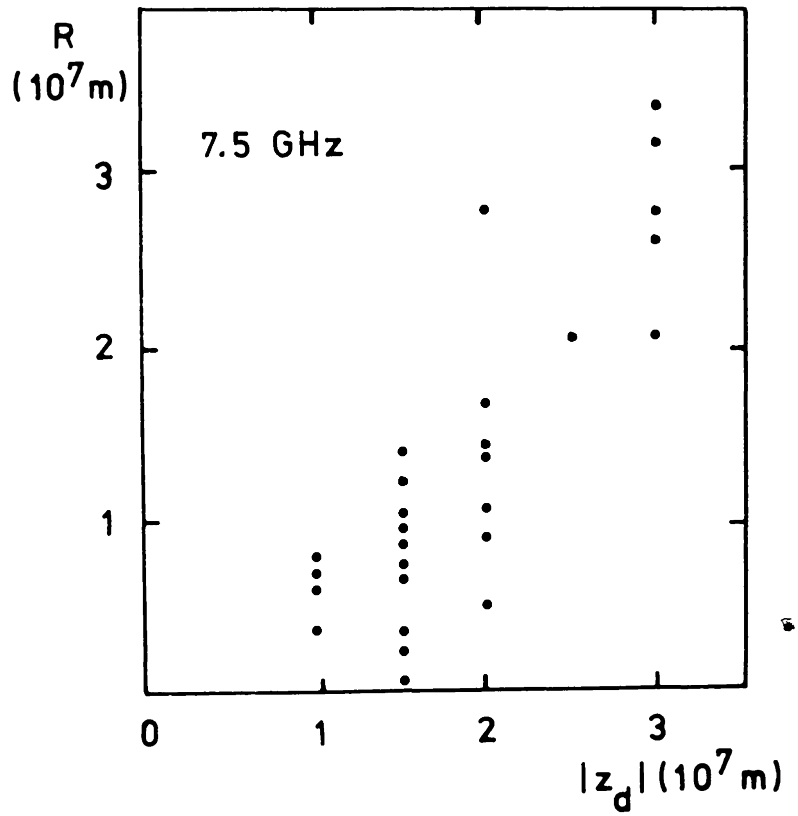

Fig. 4. Observed source radii R at 7.5 GHz in relation to the best fitting model parameters $|z_d|$ determining the magnetic scale height.

7. Relations to Flare Activity

Although the occurrence of flare instabilities may be primarily attributed to unresolved structures, we checked the significance of the present RATAN observations for a connection with flare activity. For this purpose, we compiled the flare numbers N_F (as reported in NOAA *Solar-Geophysical Data*) per active region and half solar rotation, and defined two main classes I and II according to $N_F > 40$ and $N_F \leq 40$, as well as subclasses I^+ and II^- for $N_F > 60$ and $N_F < 20$, respectively. According to these classes, mean values and standard deviations were calculated for different S-component characteristics which are shown in Table II. Hence, a tendency of increasing flux densities, source radii, and magnetic scale heights for active regions with increasing flare activity is indicated. The same tendency is much weaker marked for B_m and $\nu(p_{\max})$. The standard deviations in Table II are to be treated with caution because they merely describe the statistical error of the present sample and do not contain full information about the measuring errors, e.g., at small source sizes. Moreover, the results are influenced by the average taken from the whole active region and during a half solar rotation.

Within the framework of the above study, no clear relationship between $p_{\max}$ and the flare numbers is detectable. Analogous findings of a connection between the frequency

TABLE II

Average S-component characteristics of active regions exhibiting different degrees of flare activity (N_F, number of flares per active region and half solar rotation)

Class	I$^+$ ($N_F > 60$)	I ($N_F > 40$)	II ($N_F \leq 40$)	II$^-$ ($N_F < 20$)
$S_{v,\max}$ (s.f.u.)	12.9 ± 4.1	10.3 ± 5.3	3.4 ± 3.7	1.2 ± 1.1
$R_{7.5}$ (10^6 m)	28.4 ± 4.9	23.1 ± 8.6	15.3 ± 10.2	8.7 ± 7.1
$S_{v,\max}/R_{7.5}$	0.52 ± 0.17	0.43 ± 0.16	0.16 ± 0.13	0.10 ± 0.12
$\lvert L_B \rvert$ (10^7 m)	0.88 ± 0.23	0.80 ± 0.25	0.66 ± 0.20	0.57 ± 0.20
B_m^{obs} (T)	0.263 ± 0.052	0.250 ± 0.047	0.240 ± 0.045	0.233 ± 0.022
B_m^{calc} (T)	0.248 ± 0.033	0.240 ± 0.034	0.228 ± 0.038	0.236 ± 0.038
$\nu(p_{\max})$ (GHz)	11.0 ± 1.5	10.9 ± 1.4	9.5 ± 1.8	9.6 ± 1.9
$p_{\max}$	0.65 ± 0.30	0.62 ± 0.26	0.70 ± 0.14	0.74 ± 0.25

of X-ray bursts causing sudden ionospheric disturbances (SID-flares) and the sunspot area, but no relationship to the Mt. Wilson magnetic classes of sunspots, were reported by Achong *et al.* (1983) and Achong and Stahl (1984) although the authors later retracted their statement concerning the magnetic classes of sunspots (Sawyer *et al.*, 1985).

Large source radii and large magnetic fields and scale heights are necessary to generate sufficiently large S-component fluxes together with a 'hard' spectrum that is required, e.g., also for the well-known proton-flare criterion of Tanaka and Kakinuma (1964). Thus, the presence of a relatively large amount of magnetic flux coming into the solar corona, indicated by S-component observations, is an important factor enhancing the probability of flare activity.

The influence of the magnetic scale height is displayed in Figure 3, where averages of L_B estimated according to method 'B' are plotted versus the values $B_m/B(z)$ derived from method 'A' for several classes of active regions representing different degrees of flare activity. The plotted points agree well with the mean model characteristics and, with increasing flare activity, they are systematically shifted towards greater $\lvert L_B \rvert$ and smaller $B_m/B(z)$. The differences between the calculated (method 'B') and observed values of B_m for the above classes are generally ≤ 150 G (cf. Table II).

8. Conclusions

The present study of 36 S-component sources leads to the following conclusions:

(1) In principle, the high-resolution spectral polarimetry of microwaves together with model calculations, provides a useful tool for diagnosing active regions.

(2) Individual S-component sources reveal a wide scattering of the degree of polarization $p_{\max}$ (between about a few and hundred percent) and indicate spatially not resolved inhomogeneities.

The quantity $\nu(p_{\max})$ varies for the present sample between $\lesssim 7.5$ and 13 GHz with an average value 10.1 ± 1.8 GHz.

(3) The observations appear generally consistent with an average of both models (a) and (b). We obtain magnetic scale heights $|L_B|$ above the source centre ranging between extreme values of 0.3×10^7 and 1.2×10^7 m with an average of about 0.7×10^7 m for $z = 2 \times 10^6$ m which was checked by two different methods. These values are in general accordance with estimations by McConnel and Kundu (1984) specifying the fram earlier discussed by Dulk and McLean (1978). It should also be noted that $|L_B|$ varies (increases) with the distance r from the source centre and with height z.

(4) Corresponding to the former paragraph, the gradient of the magnetic field at $r = 0$ and $z \approx 2 \times 10^6$ m for an average S-component source is $\partial B_z/\partial z = -(0.25 \pm 0.1)$ G km^{-1}. This figure generally agrees with the gradients calculated from photospheric observations accounting for $\operatorname{div} B = 0$. Values beyond $\partial B_z/\partial z = -0.6$ G km^{-1}, as sometimes reported from optical line observations at different heights (cf., e.g., the review by Obridko, 1985), are not reproduced by the S-component observations.

(5) The tendency is proved that on an average $|L_B|$ grows with increasing source radius R of the S-component emission: generally there are no active regions with large R and small $|L_B|$ (but none vice versa, cf. Figure 4).

(6) The flare activity of active regions was found to be best correlated with the maximum flux $S_{v,\max}$ which is related to the source size and the magnetic field parameters $|L_B|$ and B_m. No obvious relation could be detected between the degree of polarization $p_{\max}$ and the flare rates (apparently coarse source inhomogeneities indicated by $p_{\max}$ do not play an essential role for the frequency of flare generation).

(7) A 'low' base of the corona above sunspots at $z \approx 2 \times 10^6$ m is consistent with the present observations (cf. also earlier approaches by Lifshitz *et al.*, 1966; Gelfreikh *et al.*, 1970; Akhmedov *et al.*, 1982, 1983; Shibasaki *et al.*, 1983).

The calculated radio and observed optical values of B_m agree within the limit of a standard deviation of ± 50 and 300 G for the average of the whole sample and the individual cases, respectively. Up to now, no clear preference can be obtained for slighly different models of the TR and of coronal temperature, and this requires further attention.

References

Achong, A. and Stahl, P. A.: 1984, *Solar Phys.* **92**, 259.

Achong, A., Stahl, P. A., and Nyak, C.: 1983, *Solar Phys.* **88**, 137.

Akhmedov, Sh. B., Gelfreikh, G. B., Bogod, V. M., and Korzhavin, A. N.: 1982, *Solar Phys.* **79**, 41.

Akhmedov, Sh. B., Gelfreikh, G. B., Fürstenberg, F., Hildebrandt, J., and Krüger, A.: 1983, *Solar Phys.* **88**, 103.

Alissandrakis, C. E., Kundu, M. R., and Lantos, P.: 1980, *Astron. Astrophys.* **82**, 30.

Bogod, V. M. and Gelfreikh, G. B.: 1980, *Solar Phys.* **67**, 29.

Chiuderi Drago, F., Bandiera, R., Falciani, R., Antonucci, E., Lang, K. R., Willson, R. F., Shibasaki, K., and Slottje, C.: 1982, *Solar Phys.* **80**, 71.

Chiuderi Drago, F. and Melozzi, M.: 1984, *Astron. Astrophys.* **131**, 103.

Dulk, G. A. and McLean, D. J.: 1978, *Solar Phys.* **57**, 279.

Gelfreikh, G. B., Akhmedov, Sh. B., Borovik, V. N., Golnev, V. Ya., Korzhavin, A. N., Nagnibeda, V. G., and Peterova, N. G.: 1970, *Izvest. Glav. Astron. Obs. v Pulkove* **185**, 167.

Gelfreikh, G. B. and Lubyshev, B. I.: 1979, *Astron. Zh.* **56**, 562.

Krüger, A. and Hildebrandt, J.: 1985, *Astron. Nachr.* **306**, 157.
Krüger, A., Fürstenberg, F., Hildebrandt, J., Akhmedov, Sh. B., Bogod, V. M., and Korzhavin, A. N.: 1983, *Publ. Debrecen Heliophys. Obs.* **5**, 619.
Krüger, A., Hildebrandt, J., Fürstenberg, F., and Staude, J.: 1982, *HHI-STP-Report, Berlin* **14**, 2.
Krüger, A., Hildebrandt, J., and Fürstenberg, F.: 1985, *Astron. Astrophys.* **143**, 72.
Kundu, M. R. and Alissandrakis, C. E.: 1984, *Solar Phys.* **94**, 249.
Lang, K. R., Willson, R. F., and Gaizauskas, V.: 1983, *Astrophys. J.* **267**, 455.
Lifshitz, M. A., Obridko, V. N., and Pikelner, S. B.: 1966, *Astron. Zh.* **43**, 1135.
McConnel, D. and Kundu, M. R.: 1984, *Astrophys. J.* **279**, 421.
Obridko, V. N.: 1985, *Sunspots and Complexes of Activity*, Nauka, Moscow, p. 119 (in Russian).
Sawyer, J. A., Achong, A., and Stahl, P. A.: 1985, *Solar Phys.* **98**, 193.
Schmahl, E. J., Kundu, M. R., Strong, K. T., Bentley, R. D., Smith, Jr., J. B., and Krall, K. R.: 1982, *Solar Phys.* **80**, 233.
Shibasaki, K., Chiuderi Drago, F., Melozzi, M., Slottje, C., and Antonucci, E.: 1983, *Solar Phys.* **89**, 307.
Solar Geophysical Data, Parts I and II, 1977–1980, US Dept. of Commerce, Boulder, Colorado.
Solnechnye Dannye, Leningrad, 1977–1980.
Staude, J.: 1981, *Astron. Astrophys.* **100**, 284.
Tanaka, H. and Kakinuma, T.: 1964, *Rep. Ionosph. Space Res. Japan* **18**, 32.